Research Article

Booramurthy Deeban, Jaganathan Maniraj*, and Manickam Ramesh

# Experimental investigation of properties and aging behavior of pineapple and sisal leaf hybrid fiber-reinforced polymer composites

https://doi.org/10.1515/epoly-2022-8104
received November 26, 2022; accepted January 02, 2023

**Abstract:** Using plant leaf fibers as reinforcements in thermo-plastic resins to produce affordable and lightweight composites is the subject of growing interest in research. Although these fibers have several advantages over synthetic fibers, mechanical characteristics of composites such as moisture absorption, poor wettability, and insufficient adhesion between the matrix and the fiber cause disadvantages. To overcome these issues, in this experimental study, two leaf-based plant fibers are hybridized and the composites have been fabricated by hand lay-up process. The composites were subjected to several tests. The results showed that the hybridization of sisal and pineapple leaf fiber (PALF) increases the mechanical strength of the composite by a maximum tensile strength of 3.59 kN, a little lower flexural strength than the individual fiber, and a noticeably higher compressive strength. The results further showed that the decreased affinities for moisture content and the aged composites seem to be prone to be hydrophilic. Findings of the experiments reveal that the hybridization of sisal and PALF has a significant influence on the properties of the composites. The scanning electron microscopy micrographs of fractured surfaces have been examined, and the findings have effectively been investigated.

**Keywords:** natural fibers, hybrid composites, hand lay-up, mechanical properties, Fourier-transform infrared spectroscopy

## 1 Introduction

Due to the rapidly increasing effect of environmental pollution, the use of fiber-reinforced polymer composites and the demand for the material offended durability and various physical and chemical properties (1,2). Synthetic fibers, along with artificial resin, stood in the frontline for decades because of their higher strength and stiffness but had created problems related to environmental concerns (3,4). Several researchers worked on replacing synthetic fibers to resolve severe problems such as renewability, health hazards, and biodegradability (5–7) caused by them. A suitable alternative for synthetic reinforcement is expected in near future as natural fibers have gained attention recently (8,9). These fibers are formed naturally and are associated with plants (hemp, sisal, pineapple, banana, coir, palm, flax, jute, etc.) and animals (sheep wool, camel, goat, rabbit, and silk moths) in large amount (10–12).

The plant-based natural fibers can produce composites with better properties as well as these materials are cost-effective, biodegradable, and readily available (10,13,14). However, the combined nature of fibers indulged with fillers will enhance the material's properties to a higher level in all aspects, such as tensile strength, stiffness, resistance to chemical substances, and thermal resistances (15–17). The higher moisture absorption and poor compatibility of plant fibers have forced the researchers to hybridize with other plant or filler or conventional fibers (18,19). The combined constituent material will always withstand its own identities, perfectly holding each other. The composite materials have more adverse properties than other materials acting alone (20,21), for example, pineapple/flax fibers reinforced with peanut oil cake showed improved tensile, flexural,

* **Corresponding author: Jaganathan Maniraj,** Department of Mechanical Engineering, KIT – Kalaignarkarunanidhi Institute of Technology, Coimbatore 641402, Tamil Nadu, India, e-mail: maniraj_j@rediffmail.com
**Booramurthy Deeban:** Department of Aeronautical Engineering, KIT – Kalaignarkarunanidhi Institute of Technology, Coimbatore 641402, Tamil Nadu, India
**Manickam Ramesh:** Department of Mechanical Engineering, KIT – Kalaignarkarunanidhi Institute of Technology, Coimbatore 641402, Tamil Nadu, India

impact, and bending strengths (22). The hybrid sisal/pineapple fibers combined with filler will reduce weight, whereas silica as fillers will strengthen the mechanical behavior of composites (23). With the enhanced high-density deposition rate and excellent adhesion qualities, the alkali-treated pineapple leaf fiber (PALF) with 3 wt% fillers increased the tensile strength by 16% and the flexural strength by 23.11%. Extended ultrasonication hours can get rid of the agglomerations. On the other hand, the failure surface morphology to the reinforcement transforms pure epoxy's glassy and multi-crack behavior by employing hand lay-up (24).

PALF has bridged the micro-level gap between two fibers by adding particles up to 7.5% of the weight fraction. These attributes result in increased flexural strength of 30.30%, tensile strength of 20.38%, compressive strength of 29.87%, and hardness of 66%. However, the material became brittle at 10% particle loading and lost binding strength. The inclusion of PALF particles in composites improves thermal stability and water absorption, resulting in increased biodegradability (25). PALF combined with viscose has an average tensile strength of 20.7 MPa, a bending strength of 23.5 MPa, and a bending modulus of 717.6 MPa. Since viscose is the main factor contributing to diminishing tensile strength, addition of PALF had improved it. Due to the inappropriate distribution of the epoxy resin, Young's modulus also decreased. As PALF/viscose yarn exhibits uniform distribution, excellent mechanical properties, and anti-moist absorption, it is used to make shopping bags, fancy roof covers, coffee cups, coffee cans, etc., giving it more excellent mechanical properties and anti-moist absorption (26).

The PALF exhibited excellent reinforcing characteristics with epoxy resin. PALF has 61.2% better tensile strength and 49.5% higher tensile modulus than coir. This primarily attributable to the fiber's 82% cellulose content and reduced micro-fibrillar angle, which promote maximum fiber/matrix attachment and increase surface roughness. As a result, materials are used in vehicle components, electrical packages, and building construction (27). Due to high bonding strength, the PALF demonstrated decreased specific wear rate and anti-slip properties when compared to other plant fibers. The inclusion of 40 wt% $TiO_2$ filler during processing is primarily responsible for the characteristics of the composites. As a result, low wear characteristics between 20 and 40 wt% was obtained, and the Taguchi technique demonstrated that PALF offers the optimal conditions for wear and frictional applications. Sisal/PALF hybrid fiber with the addition of $TiO_2$ demonstrated a lower wear rate of 500 m at a sliding distance of 1 $m \cdot s^{-1}$. A load of 5 N applied at this sliding speed resulted in considerable improvements in tensile, flexural, and impact properties. Therefore, these hybrid fiber-reinforced composites exert a significant impact on the tribological nature (28). In the present investigation, PALF and sisal leaf fiber-reinforced hybrid composite materials were fabricated using a hand lay-up process. The prepared composite materials were tested and characterized to identify their strength and characteristics. Findings of the experimental results show that the hybridization of sisal and PALF has a significant influence on the properties of composites and ascertained that these fibers could be the novel reinforcements for polymer-based composites.

# 2 Materials and methods

## 2.1 Materials

The materials used for composite fabrication such as epoxy resin (type: LY 556) and polyamine hardener (type: HY 951) were procured from a Private Company in Coimbatore, Tamil Nadu, India. The PALF and sisal fibers used as reinforcement for the composite processing were collected from the villages situated in Salem District of Tamil Nadu, India. The collected fibers were cut into the desired size, washed with water three times, and stored in an air-tight container for drying in open sunlight. Then, the fibers were treated using NaOH solution for 3 h to enhance the fibers' surface texture. From the NaOH, solution fibers were taken out, then washed with deionized water and kept for drying up to 4 h. In this experimental study, the matrix and hardener were added in the stoichiometric ratio of 10:1.

## 2.2 Processing of composites

The preparation of hybrid composites was done through the hand lay-up method. The required amount of epoxy resin and polyamine hardener was taken into a glass beaker, stirred well using a magnetic stirrer at room temperature for 4 min, and left for 60 s to achieve a proper mix. The obtained mixture was in a semi-solid state. After 1 min, the liquid state broke the bonds between resin molecules and bonded with the hardener through adhesive force. In order to protect the mold, wax material was applied on the surface, and the bottom surface was covered with a polythene sheet. The fibers were added to this mixture to produce a composite at room temperature.

This matrix and hardener are cured at room temperature. The processing of composites (from the mold to the fabricated laminate) is presented in Figure 1.

# 3 Experimental

## 3.1 Mechanical properties

The effect of fiber loading on hybrid composites was investigated through mechanical testing such as tensile, compression, flexural, and impact tests. In this experimental study, the hybrid composites have been prepared by reinforcing PALF and sisal fibers using the hand lay-up method. Mechanical tests such as tensile, flexural, compressive, and impact strength tests were conducted by using the specimens prepared as per American Society for testing and materials (ASTM) standards.

### 3.1.1 Tensile test

Tensile strength is increased during the transfer of matrix in a uniformly distributed manner with that of the fiber periodically. The tensile strength of the composite increases basically due to the enhancement in adhesion between the fiber and the matrix. The response toward decreasing tensile strength is observed at the interface between the matrix and the fiber because of the van der Waals forces that lead to improper bonding (29). The test was conducted by using a universal testing machine (UTM) with a cross-head speed of 0.5 mm·min$^{-1}$, the stress–strain curve was obtained from the machine by applying a load of 100 kN, and the load was gradually increased to 600 kN. The ASTM standard used for tensile testing is ASTM D3039. The ability to resist breaking under tensile stress is one of the most important and widely measured properties of the material and its structural applications.

### 3.1.2 Flexural test

Flexural strength is also known as a modulus of elasticity, or fracture strength of the material is defined as a material's ability to resist deformation under load (30). The flexural test was conducted using the same UTM according to the ASTM D638 standards. The test is conducted as per the following specifications:

- Maximum cross-head speed: 1 mm·min$^{-1}$,
- Support span length: 100 mm,
- Mode of test: three-point bending flexural test.

### 3.1.3 Compression test

This test was conducted on composites to obtain the average compressive strength. A laboratory experiment tested the compressive strength of a hybrid PALF and sisal fiber-reinforced epoxy composites. Axial compression loading was applied to the prepared specimen using the same UTM. The specimens were manufactured as per the ASTM D695 standards. To obtain the compression test result, the specimen is inserted into the test fixture, which is positioned between the plates of the testing machine and loaded in compression. After the specimen failed, the UTM testing system reported the maximum load that was reached.

### 3.1.4 Impact test

Izod impact test specimens with specifications of 65 mm × 13 mm × 3.2 mm and V-shape notch were fabricated in adherence to the ASTM D256 standards. Specimens were impact tested using the Tinius Olsen Impact 104 machine, and the results were reported. Three samples are tested in each case, and the average values are used for the analysis.

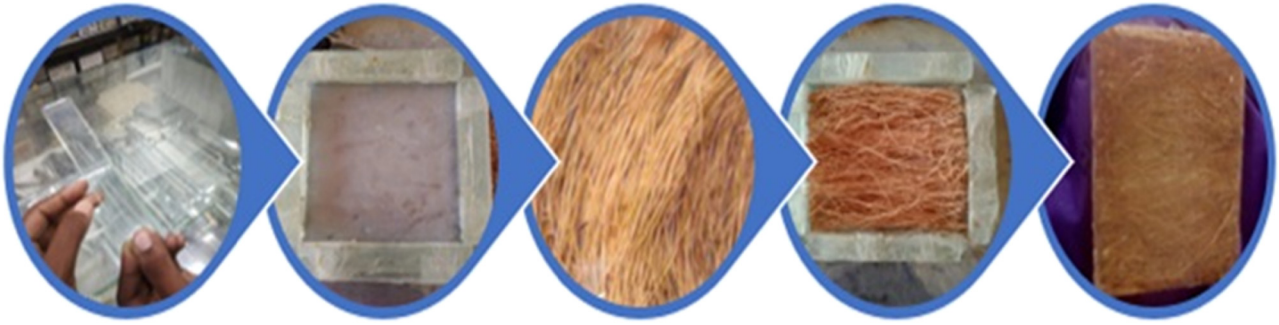

**Figure 1:** Processing of composites.

### 3.2 Water absorption studies

The volume of water absorbed during the preliminary treatment was estimated using a moisture absorption test (31). Then, it is immersed in water at a constant room temperature for 24 h. To find out the water absorption percentage, composite samples were placed in a tray full of distilled water, and the weight gain percentage is calculated by Eq. 1. The sample dimensions were taken as per the ASTM D570 standards.

$$\% \text{ Weight gain} = \frac{m_f - m_i}{m_i} \times 100 \quad (1)$$

where $m_f$ is the final weight and $m_i$ is the initial weight of the samples.

### 3.3 Fourier-transform infrared spectroscopy (FTIR) analysis

A chemical substance covered the composite surface, and its functional group was examined using an FTIR analysis (32). In this experimental study, functional groups were examined in the infrared range between 400 and 4,000 $cm^{-1}$, carried out by using Perkin Elmer Spectrum 100 FTIR instrument.

### 3.4 X-ray diffraction (XRD) analysis

The physical structure of PALF and sisal fiber composites was evaluated by XRD technique (22). In this experiment, X-ray diffractograms were obtained with the condition used where CuKα (wavelength 1.54 Å) ($2\theta \cdot 5\ s^{-1}$), scanning values of $2\theta$ ranging from 10° to 70°. The X'pert Pro model instrument was used for identifying the crystalline phase, which is a PAN analytical 3. The crystallinity index (CI) was calculated using Eq. 2, and the crystallite size is calculated using Scherrer's formula, given in Eq. 3 (33).

$$CI = (H_{22.55} - H_{18.5})/H_{22.55} \quad (2)$$

where $H_{22.55}$ and $H_{18.5}$ are heights of the X-ray spectrum peak at a Bragg's angle of 22.55 and 18.5, respectively.

$$CS = \frac{K\lambda}{\beta COS\theta} \quad (3)$$

where $K = 0.89$ is Scherrer's constant, $\beta$ is the width of the peak at half maximum, $\lambda$ is the wavelength of the radiation, and $\theta$ is Bragg's angle.

### 3.5 Scanning electron microscopy (SEM) studies

The morphological behavior of the fractured surfaces of the PALF and sisal fiber-reinforced hybrid composite and the energy imparted during the loading of fibers absorbed by cellulose and its ability were analyzed with the help of the SEM analysis. The scanning of samples was carried out by using the electron microscope of model JSM 6360LA, JOEL, made in Japan.

## 4 Results and discussion

### 4.1 Mechanical behavior

The experimental results obtained from mechanical testing are tabulated in Table 1. To finalize the average values of the composite, a total of three samples were tested and the test was conducted at room temperature. Figure 2 shows the strength comparisons of different composite materials obtained from PALF and sisal fibers subjected to mechanical loading. The results indicated that hybridization plays a significant role in determining the strength of the composites.

#### 4.1.1 Tensile strength analysis

The analysis of the tensile test results is presented in Figure 2. From the analysis, it is found that the tensile

**Table 1:** Mechanical properties of the composites

| Composite sample | Displacement (mm) | Tensile strength (kN) | Compressive strength (kN) | Flexural strength (kN) | Impact strength ($N \cdot mm^{-2}$) |
|---|---|---|---|---|---|
| PALF | 2.3 | 1.46 | 2.37 | 1.77 | 44 |
| Sisal | 3.5 | 2.49 | 1.83 | 1.41 | 43.5 |
| Hybrid | 3 | 3.59 | 3.63 | 1.65 | 43 |

strength values were not the same for all the samples and differed based on the cross-sectional area and elongation. The tensile strength of the PALF and sisal fiber-reinforced hybrid composites is found to have a maximum of 1.46, 2.49, and 3.59 kN due to their cellulose content and fiber bundling characteristics. Similarly, it is observed that only PALF-reinforced composites exhibit lower tensile strength because of the presence of voids in the composite material. The response to tensile failure is mainly influenced by the fiber pullout and the presence of cracks. The strength of PALF is around 80 N, and the diameter is between 0.3 and 0.4 mm. The mechanical properties of sisal fiber 9–38 GPa, elongation of 18.2%, and average tensile strength of 1,090 $N{\cdot}mm^{-2}$ was obtained.

#### 4.1.2 Flexural strength analysis

The flexural strength variation between the composites is studied to understand the bending ability of the composite, which is shown in Figure 2. From the figure, it is observed that the flexural strength of the composites is increased by increasing the fiber loading with the matrix. It is also observed that the flexural strength is reduced due to the interaction between fibers upon increasing the fiber loading. Observations reveal that macromolecules' movement within the matrix and the fiber enhances the flexural strength. This provides resistance to the initiation of crack formation in the composite. The higher diffusion rate between the fiber and the matrix tends to tighten in both PALF and sisal fibers where it seems to withstand heavy load. The reduction in flexural strength of sisal fiber composite was due to the presence of kink in the source of fiber.

#### 4.1.3 Compressive strength analysis

The compressive load variation among the composites is shown in Figure 2. The composite's restoring ability is also known after being released from the addition of loads. Similarly, composite resistance to compression loading is also determined. From the results, it is found that the ultimate compression strength of PALF composite is 2.37 kN, that of sisal fiber composite is 1.82 kN, and the hybrid composites hold the maximum compressive strength of 3.63 kN. It is demonstrated that there is dissimilarity in compression loading among the tested composite samples. The obtained results elaborately provide a keen display that these hybrid composites withstand high load comparatively with that of other plant fiber composites, which is due to the transverse delamination because of the addition of external forces over the composite tending to move toward failure mode.

#### 4.1.4 Impact strength analysis

The hybrid composite's impact strength is determined to be average when compared to PALF and sisal fiber-

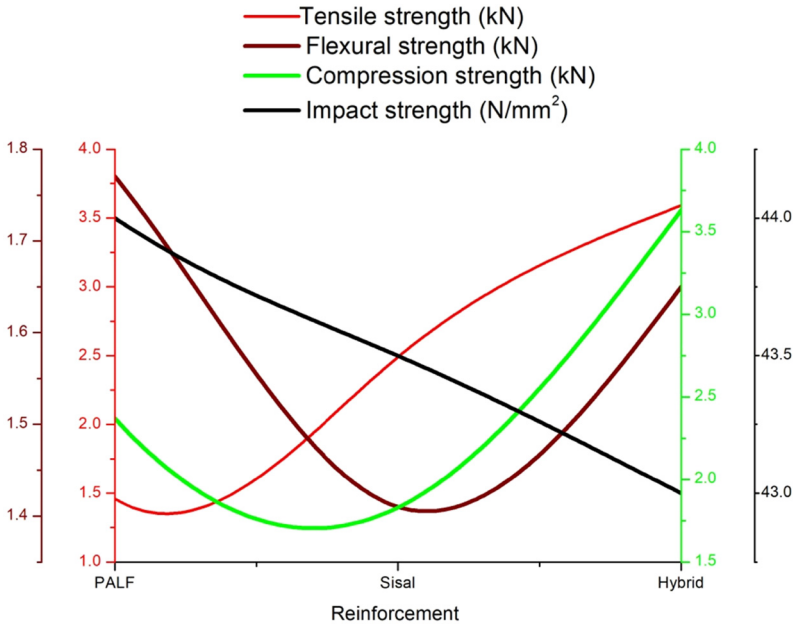


**Figure 2:** Mechanical strength of the PALF, sisal, and hybrid composites.

**Table 2:** Water absorption behavior of various composites

| S. no | Sample | % Weight gain for fresh epoxy composites (g) | | % Weight gain for 1-year-aged epoxy composites (g) | |
|---|---|---|---|---|---|
| | Temp of water | 24 h 28.3°C | 48 h 28°C | 24 h 28.3°C | 48 h 28°C |
| 1. | PALF | 1.82 | 1.79 | 3.70 | 3.70 |
| 2. | Sisal | 2.04 | 5.77 | 4.17 | 2.08 |
| 3 | Hybrid | 1.67 | 2.44 | 3.73 | 3.56 |

reinforced composites separately. The sisal fiber-reinforced composites have been demonstrated to have lower strength than PALF composites. In this experiment, the fibers are reinforced in a longitudinal orientation. The primary reason for the poor impact strength is the weak interfacial connection between the matrix and the fiber, which is confirmed from SEM images. There are no significant changes seen in the PALF/sisal hybrid composite.

## 4.2 Water absorption property analysis

The increase in weight of the samples depends on the amount of water absorbed by the samples, which was determined based on the initial weight. The sample's porosity induces absorption of a relatively higher amount of water. The adequate porosity level in fiber holds to gain higher water content compared to lower pore capacity of the sample, which is holding lower water content. The water absorption property of the composites is shown in Table 2, representing the percentage of weight gain of the individual sample based on time and year, maintaining a constant temperature. Initially, all the samples were kept in water, and absorption rate increased gradually and reaching the saturation limit. It is observed that the composites' increment in weight for 24 h at 28.3°C, and 48 h at 28°C, as shown in Figure 3a.

The percentage increase in weight of PALF shows better absorption property concerning epoxy resin. It has been observed that the epoxy aged 365 days shows a greater absorption property than newly procured one. It is identified that the PALF and sisal fibers are hydrophilic, due to which the absorption rate is higher upon holding epoxy resin, as shown in Figure 3b. This, in turn, develops micro-cracking in the composite turning to reduce the brittleness of the resin. With the effect of micro-cracking, the fiber's swelling develops, leading to the failure of the matrix. It holds the easy pathway for water molecules to absorb through the capillary effect.

## 4.3 FTIR analysis

The spectral difference between the sisal fiber and PALF composite is shown in Figure 4. The presence of the O–H stretching vibration is due to the strong absorption of the hydroxyl group at 3,477 $cm^{-1}$, possibly for all cellulose fibers. The C–H stretching vibration leads to a weak position noted at 2,916 $cm^{-1}$. The strong position is due to the bending vibration of C–H almost holding a strong absorption peak at 1,649 $cm^{-1}$. The occurrence of lignin and hemicellulose, as well as wax, primarily originates in plants. Moreover, during the alkalization process, all are removed, whereas, in the crystalline, cellulose is

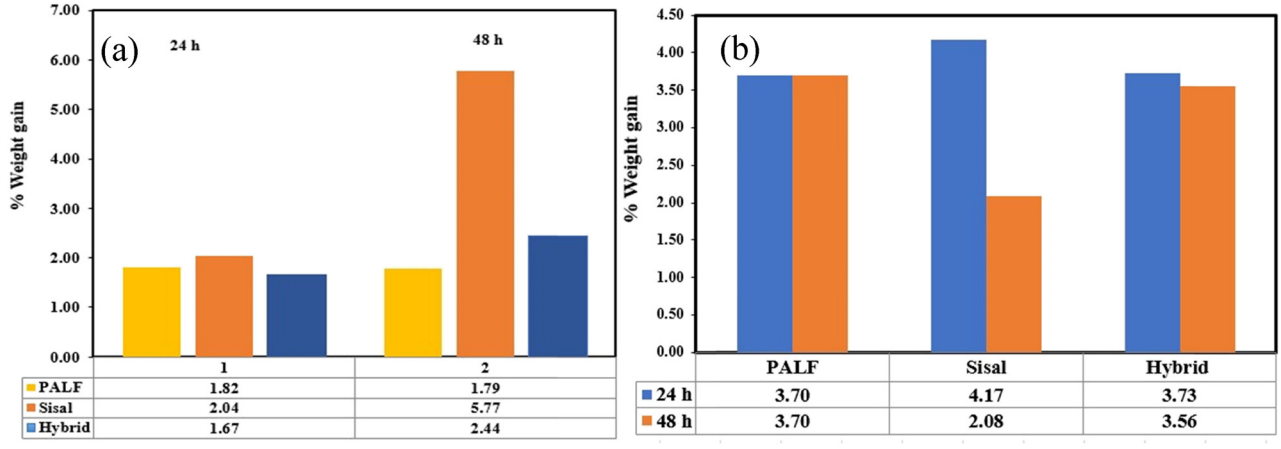


**Figure 3:** Water absorption nature of (a) fresh epoxy composites and (b) 1-year-aged epoxy composites.

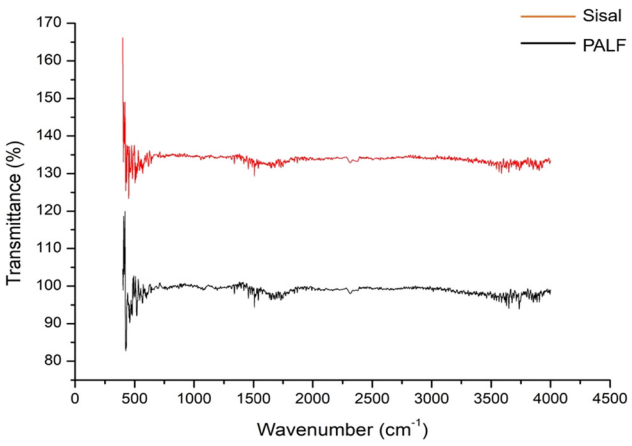


**Figure 4:** FTIR pattern of PALF and sisal fiber composites.

identified in the peak range of 1,419, 1,132, and 887 $cm^{-1}$. There is also a transformation between the cellulose molecules internally all over the bands. The figure further indicates the PALF composite confirm the strong absorption peak at 3,441 $cm^{-1}$ due to the hydroxyl group emerging over the surface. The stretching vibration due to C═O is attributed to the presence of hemicellulose indicated at 1,691 $cm^{-1}$ and slowly decreased. Removal of lignin, wax, and oil from fibers is carried out during treatment with NaOH, which are identified at 1,460 and 2,895 $cm^{-1}$.

The result of FTIR for the PALF composite indicates the presence of hemicellulose and lignin in the peak of 1,753 $cm^{-1}$. Then, the usual appearance of the hydroxyl group has a stretching vibration at 3,452 $cm^{-1}$. The peak attributed to bending vibration holding cellulose molecules is at 1,060 $cm^{-1}$. The cellulose particles show asymmetrical stretching at 1,110 $cm^{-1}$ and the deformation of the particles along with C–O and C–H at 1,384 and 1,410 $cm^{-1}$. The effectiveness of the fiber content with high-level cellulose content is seen through alkaline treatment. In sisal fiber composite, the presence of hydroxyl group is noted at 3,440 $cm^{-1}$, confirming a stretching vibration and the presence of a band with a C═O group. The presence of tetrahedral is due to the absorption developed over the surface of the composite, which is observed in the peak range of 1,506–1,626 $cm^{-1}$. The C–O stretching vibration is observed at 1,247 $cm^{-1}$. The peak range between 549 and 586 $cm^{-1}$ represents the presence of apatite formed over the surface of the composite.

## 4.4 XRD analysis

The crystalline phase was identified through XRD analysis of the composites. The composite is scanned in the $2\theta$ range between 10° and 50°. The occurrence of diffraction peaks is in the specified range located at different angles. The peak value concerning the presence of the rutile phase at 29.97°, 36.43°, 39.82°, 47.97°, and 49.04°, indicating that particles are amorphous and rely on the crystalline region, is shown in Figure 5. These peak values coincide with the Joint Committee of Powder Diffraction Standards data of numbers 88-1175 and 84-1286. The level of amorphous in such a way that the crystalline diffraction level is increased due to the treatment of fiber surface by alkaline solution.

The diffraction peaks are at 14.6°, 16.3°, 20.8°, and 22.9°, indicating that due to alkaline treatment, the crystalline property has been enhanced by lowering the non-crystalline substances. It is also evidenced that a larger crystalline size lowers fibers' hydrophilic properties and enhances the composite's mechanical properties. The broad peaks of the diffraction pattern were identified at 15.68°, 16.2°, 20.3°, 23.01°, and 30.2°. The composite layers seem to be very strong and sharp, providing an extensive apatite layer formation over the surface. It is observed that the CI gradually increased due to the alkaline treatment, which in turn reduces the amorphous part of the cellulose in the fiber. The interpretation of the peaks showed that the observed pattern with the individual visible peaks is broad and the intensity between peaks results from peak overlap, which is determined from the Segal method.

## 4.5 SEM analysis

SEM images indicate the morphological behavior of the composite materials obtained from various samples and

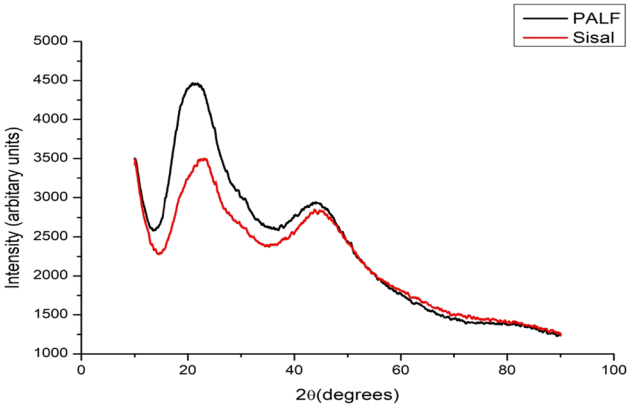


**Figure 5:** XRD analysis of PALF and sisal fiber composites.

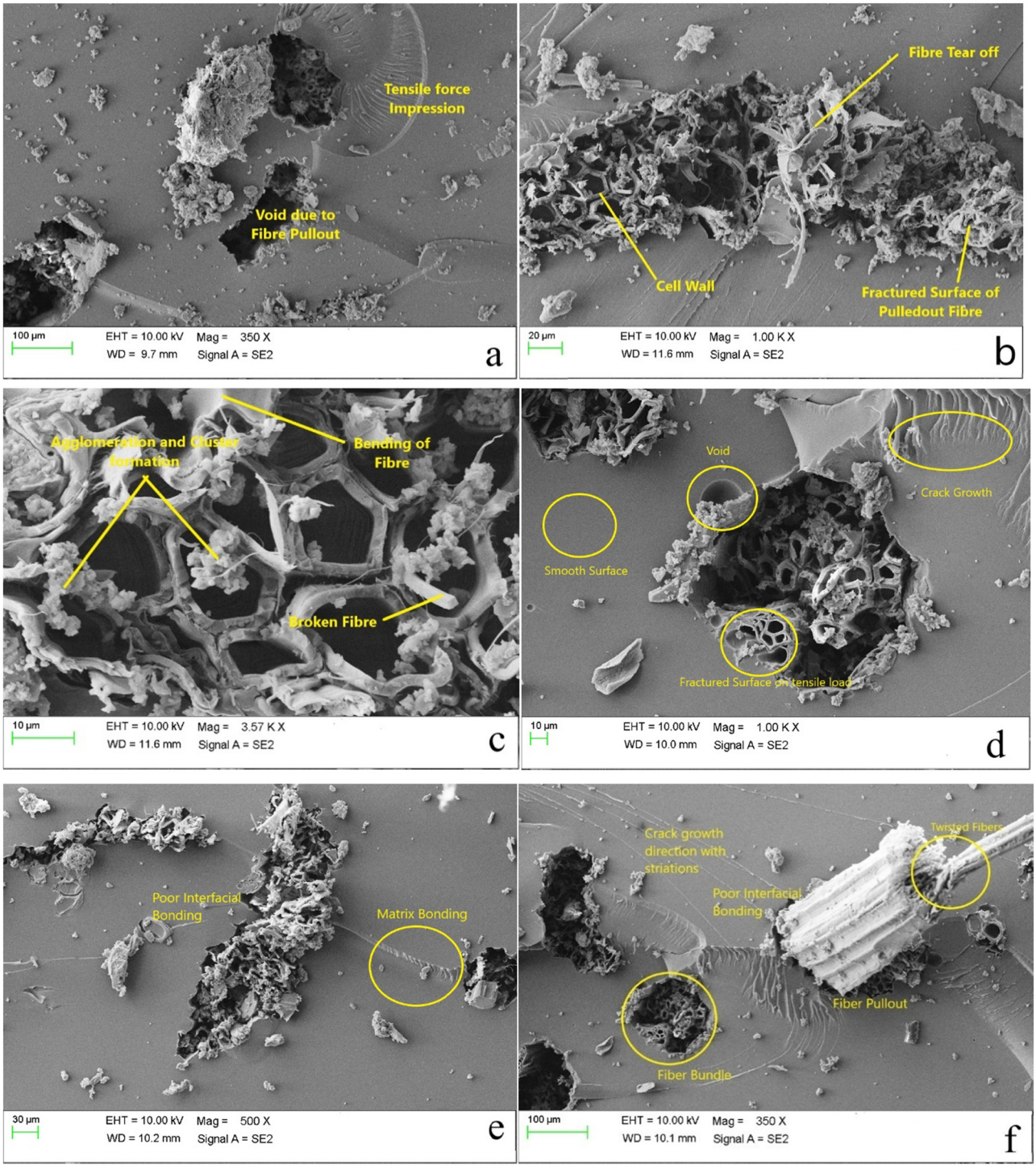


**Figure 6:** SEM images of fractured surfaces of PALF composite subjected to: (a) tensile loading, (b) compressive loading, (c) flexural loading and sisal fiber composite subjected to: (d) tensile loading, (e) compressive loading, and (f) flexural loading.

were discussed concerning the observations reported. Figure 6a–c shows the PALF composite-fractured surface, which ultimately occurred because of tensile and flexural loading. The reduction in hemicellulose upon alkaline treatment is also confirmed. The surface of the composite is smooth with visible pores. The fiber pull-out, fiber tear-off, parallel fiber cracks, broken fiber, and agglomeration of fibers have also been witnessed from SEM images. As for Figure 6d–f, the sisal fiber composite sample failure and fracture during the mechanical loading adversely

affect the cellulose molecule. Eventually, it happens due to the cellulose molecule's enormous impact on energy absorption. The failure will occur in some circumstances because of improper stress distribution, which affects the agglomeration of the particles. It shows that the cellulose pull-out is the evidence of composite failure, which may depend on the cellulose concentration (lower or higher). It also indicates that traces of fiber pull-out present in the fractured surface occurred on the surface of the sisal fiber composite. The formation of agglomeration will reduce mechanical strengths by holding improper bonding at the interface between the fiber and the matrix. The confirmation prevails that the bonding between the fiber and the matrix is low because of the poor intermolecular attraction force, leading to textural fracture.

## 5 Conclusion

In this experimental study, the PALF, sisal, and hybrid composites were fabricated by the hand lay-up technique and the various characteristics and behaviors of the composites were examined. From the results, it is found that mechanical properties of sisal and PALF hybrid composite have a tensile strength of 3.59 kN, which is higher than that of the individual sisal fiber and PALF composites. The PALF/sisal hybrid fiber-reinforced composite had a better flexural strength of 1.65 kN, which is intermediate between the PALF (1.77 kN) and sisal (1.41 kN) fiber-reinforced composites. It is also seen that sisal fiber combined with PALF reduces the overall flexural strength up to 0.12 kN, which is the minimum value that will not make the structure flexurally weak. The compression strength is higher in the hybrid composites than in the other two individual fiber-reinforced composites. The impact strength of the hybrid composites has been found low due to the poor interfacial bonding between the matrix and the fiber. The enhancement in mechanical property reduced the affinity toward moisture content. The alkaline treatment increases the surface area and roughness of the composites.

This study reveals that PALF-reinforced epoxy composites provide an excellent water absorption property compared to sisal fiber-reinforced composites, whereas the difference has a slight variation. The water absorption property tends to be higher in the case of PALF showing a higher concentration of cellulose molecules, whereas the sisal contains the lower value holding a lower concentration of cellulose molecules. The FTIR results confirm the strong absorption peak at 3,441 $cm^{-1}$ due to the hydroxyl group emerging over the PALF surface. The presence of tetrahedral due to the absorption developed over the surface of the sisal fiber is also observed in the peak range of 1,506–1,626 $cm^{-1}$. The XRD peak values show the presence of the rutile phase at 29.97°, 36.43°, 39.82°, 47.97°, and 49.04°, indicating that particles are amorphous and rely on the crystalline region. Both PALF and sisal fibers possess a similar surface morphology without significant modification, which is observed from SEM images. Some of the defects, such as the bonding interface between the fiber and the matrix, show a poor intermolecular attraction that influences the mechanical strength.

**Funding information:** The authors state no funding involved.

**Author contributions:** Booramurthy Deeban: writing – original draft, methodology, formal analysis; Jaganathan Maniraj: writing – original draft, formal analysis, visualization; Manickam Ramesh: writing – review and editing, supervision, resources.

**Conflict of interest:** The authors state no conflict of interest.

## References

(1) Goulis P, Kartsonakis IA, Mpalias K, Charitidis C. Combined effects of multi-walled carbon nanotubes and lignin on polymer fiber-reinforced epoxy composites. Mater Chem Phys. 2018;218:18–27.
(2) Sahayaraj AF, Muthukrishnan M, Ramesh M. Experimental investigation on physical, mechanical, and thermal properties of jute and hemp fibers reinforced hybrid polylactic acid composites. Polym Compos. 2022;43:2854–63.
(3) Soni S, Rana RS, Singh B, Rana S. Synthesis and characterization of epoxy based hybrid composite reinforced with glass fiber and milled carbon. Mater Today Proc. 2018;5:4050–8.
(4) Rangappa SM, Siengchin S, Parameswaranpillai J, Jawaid M, Ozbakkaloglu T. Lignocellulosic fiber reinforced composites: Progress, performance, properties, applications, and future perspectives. Polym Compos. 2022;43(2):645–91.
(5) Arun M, Vincent S, Karthikeyan R. Development and characterization of sisal and jute cellulose reinforced polymer composite. Mater Today Proc. 2020;28:556–61. doi: 10.1016/j.matpr.2019.12.218.
(6) Ramesh M, Tamil Selvan M, Niranjana K. Thermal characterization and hygrothermal aging of lignocellulosic *Agave Cantala* fiber reinforced polylactide composites. Polym Compos. 2022;43:6453–63.
(7) Sahayaraj AF, Muthukrishnan M, Ramesh M. Influence of *Tamarindus indica* seed nano-powder on properties of *Luffa cylindrica* (*L.*) fruit waste fiber reinforced polymer composites. Polym Compos. 2022;43:6442–52.
(8) Seldon PA, Abilash N. Appraisal on varied natural and artificial fiber reinforced polymeric composites. Mater Today Proc. 2019;22:3213–9.

(9) Hayajneh MT, Al-Shrida MM, AL-Oqla FM. Mechanical, thermal, and tribological characterization of bio-polymeric composites: A comprehensive review. e-Polymers. 2022;22:641–63.
(10) Sanjay MR, Siengchin S, Parameswaranpillai J, Jawaid M, Pruncu CI, Khan A. A comprehensive review of techniques for natural fibers as reinforcement in composites: Preparation, processing and characterization. Carbohydr Polym. 2019;207:108–21.
(11) Vigneshwaran S, Sundarakannan R, John KM, Joel Johnson RD, Prasath KA, Ajith S, et al. Recent advancement in the natural fiber polymer composites: A comprehensive review. J Clean Prod. 2020;277:124109.
(12) Ramesh M, Deepa C, Rajeshkumar L, Tamil Selvan M, Balaji D. Influence of fiber surface treatment on the tribological properties of *Calotropis gigantea* plant fiber reinforced polymer composites. Polym Compos. 2021;42:4308–17.
(13) Sarikaya E, Çallioğlu H, Demirel H. Production of epoxy composites reinforced by different natural fibers and their mechanical properties. Compos Part B Eng. 2019;167:461–6.
(14) Bhoopathi R, Ramesh M. Influence of eggshell nanoparticles and effect of alkalization on characterization of industrial hemp fibre reinforced epoxy composites. J Polym Env. 2020;28:2178–90.
(15) Ojha AR, Biswal S. Thermo physico-mechanical behavior of palm stalk fiber reinforced epoxy composites filled with granite powder. Compos Commun. 2019;16:158–61.
(16) Yan L, Chouw N, Jayaraman K. Flax fibre and its composites – A review. Compos Part B. 2014;56:296–317.
(17) Ramesh M, Rajeshkumar L, Srinivasan N, Vasanth Kumar D, Balaji D. Influence of filler material on properties of fiber reinforced polymer composites: A review. e-Polymers. 2022;22:898–916.
(18) Gupta MK, Ramesh M, Thomas S. Effect of hybridization on properties of natural and synthetic fiber-reinforced polymer composites (2001–2020): A review. Polym Compos. 2021;42:4981–5010.
(19) Sahari J, Maleque MA. Effect of oil palm ash on the mechanical and thermal properties of unsaturated polyester composites. e-Polymers. 2016;16(4):323–9.
(20) Gopal Krishna UB, Srinivasa CS, Amara NS, Gudoor S. Processing, characterization and property evaluation of seashell and glass fibre added epoxy based polymer matrix composite. Mater Today Proc. 2019;35:417–22.
(21) Neves ACC, Rohen LA, Mantovani DP, Carvalho JPRG, Vieira CMF, Lopes FPD, et al. Comparative mechanical properties between biocomposites of epoxy and polyester matrices reinforced by hemp fiber. J Mater Res Technol. 2020;9:1296–304.
(22) Sumesh KR, Kanthavel K, Kavimani V. Peanut oil cake-derived cellulose fiber: Extraction, application of mechanical and thermal properties in pineapple/flax natural fiber composites. Int J Biol Macromol. 2020;150:775–85.
(23) Sumesh KR, Kavimani V, Rajeshkumar G, Indran S, Saikrishnan G. Effect of banana, pineapple and coir fly ash filled with hybrid fiber epoxy based composites for mechanical and morphological study. J Mater Cycles Waste Manag. 2021;23:1277–88.
(24) Suresha B, Hemanth G. Effect of halloysite nanotubes on morphology and mechanical properties of alkali treated pineapple fiber reinforced epoxy composites. Mater Today Proc. 2021;46:9047–53.
(25) Saha A, Kumar S, Kumar A. Influence of pineapple leaf particulate on mechanical, thermal and biodegradation characteristics of pineapple leaf fiber reinforced polymer composite. J Polym Res. 2021;28:66.
(26) Mahmud RU, Momin A, Islam R, Siddique AB, Khan AN. Investigation of mechanical properties of pineapple-viscose blended fabric reinforced composite. Compos Adv Mater. 2022;31:263498332210877.
(27) Hoque MB, Hannan MA, Mollah MZI. Review on the mechanical properties of pineapple leaf fiber (PALF) reinforced epoxy resin based composites. Res J Eng Technol. 2021;6:855–60.
(28) Sumesh KR, Saikrishnan G, Pandiyan P, Prabhu L, Gokulkumar S, Priya AK, et al. The influence of different parameters in tribological characteristics of pineapple/sisal/$TiO_2$ filler incorporation. J Ind Text. 2022;51:8626S–44S.
(29) Sanjay MR, Arpitha GR, Yogesha B. Study on mechanical properties of natural - glass fibre reinforced polymer hybrid composites: A review. Mater Today Proc. 2015;2:2959–67.
(30) Ramesh M. Flax (Linum usitatissimum L.) fibre reinforced polymer composite materials: A review on preparation, properties and prospects. Prog Mater Sci. 2018;102:109–66.
(31) Chen J, Zou Y, Ge H, Cui Z, Liu S. Mechanical and water absorption behaviors of corn stalk/sisal fiber-reinforced hybrid composites. J Appl Polym Sci. 2018;135:46405.
(32) Soundar A, Kandasamy J. Mechanical, chemical and morphological analysis of crab shell/sisal natural fiber hybrid composites. J Nat Fiber. 2021;18:1518–32.
(33) Ramesh M, Deepa C, Niranjana K, Rajeshkumar L, Bhoopathi R, Balaji D. Influence of Haritaki (*Terminalia chebula*) nanopowder on thermomechanical, water absorption and morphological properties of Tindora (*Coccinia grandis*) tendrils fiber reinforced epoxy composites. J Nat Fiber. 2022;19(13):6452–68.